Electronic Supplementary Material (ESI) for Journal of Materials Chemistry A.
This journal is © The Royal Society of Chemistry 2018

ELECTRONIC SUPPLEMENTARY INFORMATION

Evaluation of the highly stable metal-organic framework MIL-53(Al)-TDC (TDC = 2,5-thiophenedicarboxylate) as a new and promising adsorbent for heat transformation applications

Niels Tannert,[a,x] Sebastian-Johannes Ernst,[b,c,x] Christian Jansen,[a] Hans-Jörg Bart,[b] Stefan K. Henninger[c] and Christoph Janiak[a,*]

[a] *Institut für Anorganische Chemie und Strukturchemie, Heinrich-Heine-Universität Düsseldorf, Universitätsstraße 1, 40225 Düsseldorf, Germany.*

[b] *Chair of Separation Science and Technology, TU Kaiserslautern, Postfach 3049, 67653 Kaiserslautern, Germany.*

[c] *Fraunhofer Institute for Solar Energy Systems (ISE), Heidenhofstr. 2, 79110 Freiburg, Germany.*

x These authors contributed equally.

**E-mail: janiak@uni-duesseldorf.de*

further Emails: Niels.Tannert@uni-duesseldorf.de; sebastian-johannes.ernst@ise.fraunhofer.de; christian.jansen@hhu.de; bart@mv.uni-kl.de; stefan.henninger@ise.fraunhofer.de

Keywords

Metal-Organic Frameworks, MIL-53(Al)-TDC, Synthesis Optimization, Water Sorption, Isosteric Heat of Adsorption, Cooling Performance, Multicycle stability, Hydrothermal stability, Chemical stability, Thermal stability, Heat transformation application

Table of Contents

Section S1. Chemicals
Section S2. Synthesis optimization
Section S3. Karl-Fischer titrations
Section S4. PXRD measurements
Section S5. Solvent and pH stability
Section S6. Thermogravimetric analysis (TGA)
Section S7. Elemental analysis
Section S8. Infrared spectroscopy (IR)
Section S9. Scanning electron microscopy (SEM)
Section S10: Nitrogen sorption experiments (T = 77 K)
Section S11. Argon sorption experiments (T = 87 K)
Section S12: Water sorption and isosteric heat of adsorption
Section S13: Multicycle stability tests
Section S14. References

S1. Chemicals

All chemicals were used as received by supplier (cf. Table S1).

Table S1 *Used chemicals, supplier and purities.*

Chemical	Supplier	Purity
Acetone	Sigma Aldrich	>99.5%
$AlCl_3 \cdot 6\ H_2O$	Janssen Chimica	99%
$Al(SO)_4 \cdot 18H_2O$	AppliChem	not specified
$Al(OH)(acetate)_2 \cdot x\ H_2O$	AlfaAesar	not specified
Diethylether	Riedel de Haën	99.8%
Dimethylformamide	Fischer Chemicals	99.99%
Ethanol	Chem Solute	99.9%
2,5-Furandicarboxylic acid	OxChem	95%
Hydrochloric acid, 37%	Sigma Aldrich	37%
$NaAlO_2$	VWR Chemicals	not specified
NaOH (microgranulate)	Chem Solute	not specified
Nitric acid, 65%	VWR Chemicals	not specified
Tetrahydrofuran	Riedel de Haën	p.a.
2,5-thiophenedicarboxylic acid	Sigma Aldrich	99%

S2. Synthesis optimization

The syntheses were following a modified protocol of Tschense *et al.*.[1]

Approximately 5.0 mmol of 2,5-thiophenedicarboxylic acid (H_2TDC) and 5.7 mmol of either $AlCl_3 \cdot 6\ H_2O$, $Al_2(SO_4)_3 \cdot 18\ H_2O$, $Al(OH)(ac)_2 \cdot x\ H_2O$ or $NaAlO_2$ were refluxed (24 h, 135 °C) with 32 mL of water and 8 mL of dimethylformamide (DMF). The precipitate was recovered by centrifugation, consecutively washed and re-dispersed in water (three times, 100 mL each). A fourth washing step was applied by further stirring in water (100 mL, 24 h). After final centrifugation and decantation, the product was dried under reduced pressure (24 h, 80 °C, 50 mbar). All products were obtained as white powders. Table S2 summarizes the synthesis results.

Table S2 *Synthesis results of MIL-53(Al)-TDC syntheses using different aluminum sources.*

Al-source	Reactant [g][a]	Yield [g]	Yield [%]	BET [m^2g^{-1}][b]
$Al(OH)(ac)_2 \cdot x\ H_2O$	1.027	0.983	95, 91	885, 1092
$NaAlO_2$	0.469	0.482	39	394
$Al(SO)_4 \cdot 18H_2O$	3.798	0.946	88	1102
$AlCl_3 \cdot 6\ H_2O$	1.376	0.889	83	1096
ref. [1]	1.158	0.880	84	1150

[a] The weighted amounts of $Al(OH)(ac)_2 \cdot x\ H_2O$ and $NaAlO_2$ were adjusted in terms of water content per formula unit (cf. Section S3). [b] Determined by five adsorption points of nitrogen sorption isotherms.

S3. Karl-Fischer titrations

In order to weigh out the proper stoichiometric amounts of $Al(OH)(ac)_2 \cdot x\ H_2O$ and $NaAlO_2$, which was suspected to contain water of crystallization, we carried out Karl-Fischer-titrations. Both experiments were carried out on an *ECH AQUA 40.00* (ECH, Halle (Saale), Germany) with repeated

determinations. Therefore, $Al(OH)(ac)_2 \cdot x\ H_2O$ (12.90 mg) and $NaAlO_2$ (11.00 mg) were analyzed. The water contents were determined to be 9.82% for $Al(OH)(ac)_2 \cdot x\ H_2O$ and 3.21% for $NaAlO_2$, correlating to formulas of approximately $Al(OH)(ac)_2 \cdot H_2O$ and $NaAlO_2 \cdot 0.2\ H_2O$. Hence, both molar weights were adjusted and taken into account for calculation of reactant ratios during synthesis optimizations.

S4. PXRD measurements

Powder X-ray diffraction (PXRD) patterns were obtained at ambient temperature on a *D2 phaser* (BRUKER, Billerica, US) using Cu-Kα radiation (λ = 1.54182 Å) between 5° < 2Θ < 50° with a scanning rate of 0.0125 °/s (300 W, 30 kV, 10 mA). The diffractograms were obtained on a flat "low background sample holder", in which at low angle the beam spot is strongly broadened so that only a fraction of the reflected radiation reaches the detector, hence the low relative intensities measured at 2Θ < 7°. Analyses of the diffractograms were carried out with *Match 3.11* software.

X-ray diffractograms under humid conditions were acquired *in-situ* on a *Bruker D8 Advance* with *DaVinci™* (BRUKER, Billerica, US), using a Cu anode tube at 40 kV/40 mA, with a Ni filter and constant sample illumination spot size (broadness: 12 mm); step size 0.02°, 1.0 s/step, Cu-K_α radiation. *MRI Humidity Stage* (BRUKER AXS, Karlsruhe, Germany) was used for controlled humidity, where a humidified N2 gas flow was passed over the sample at atmospheric pressure. Before each scan, the sample was allowed to equilibrate for 90 min.

All relevant PXRD plots of synthesis optimization are given in the full paper in Figure S1.

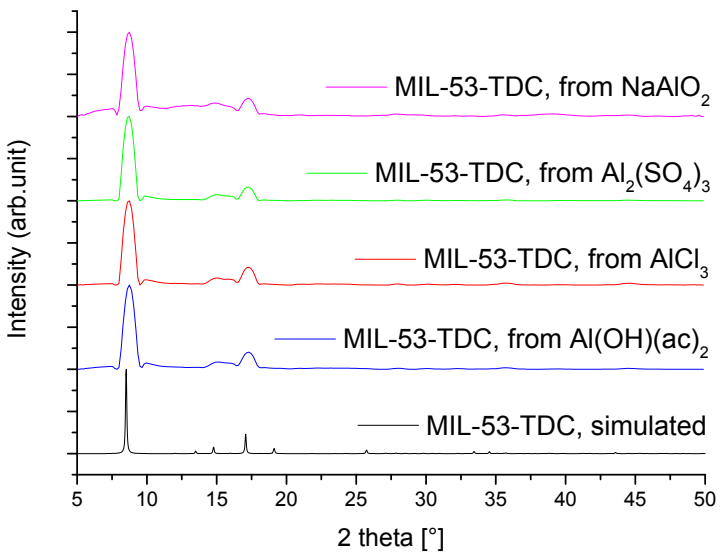

Figure S1 *PXRD patterns of different MIL-53(Al)-TDC samples obtained by varying aluminum salt sources. The theoretical powder pattern was calculated from a cif-file that was generously provided by Serre and co-workers.*

Figure S2 and **F**igure S3 show the PXRD patterns of an adsorption-desorption isotherm at 40 °C. Before and after ten cycles performed in an *in-situ PXRD* humidity chamber. As can be seen from the diffractograms, the reflexes decrease in the presence of humidity but increase reproducibly during desorption.

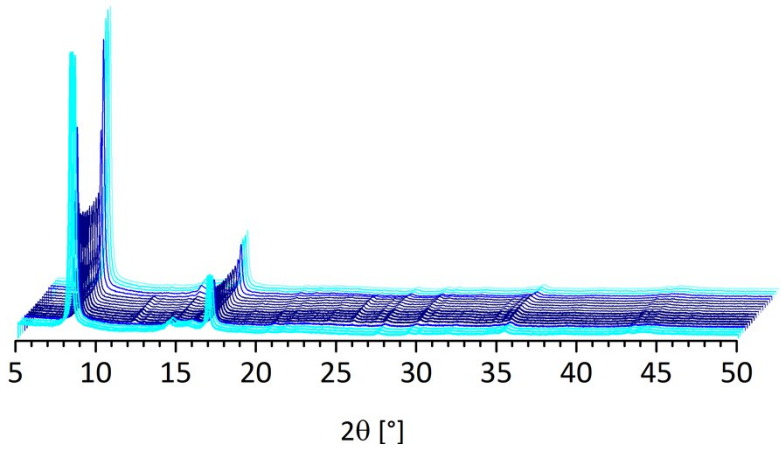

Figure S2 *Complete adsorption-desorption in-situ PXRD at 40 °C* ***before*** *the performed multicycling. Light blue represent desorbed state, whereas dark blue indicates adsorbed state.*

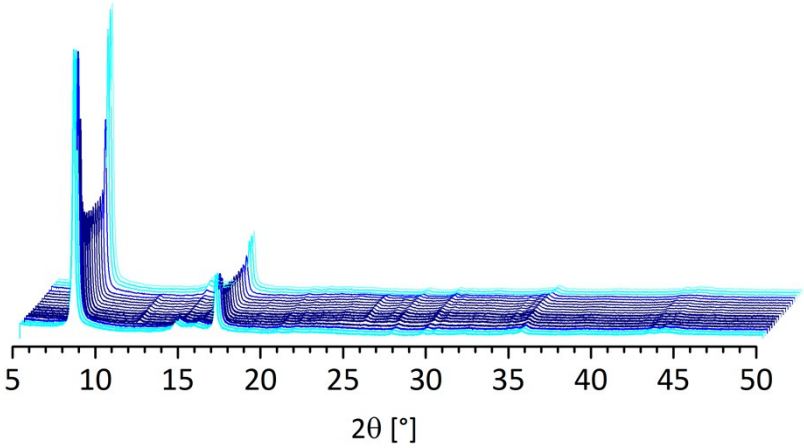

Figure S3 *Complete adsorption-desorption in-situ PXRD at 40 °C* ***after*** *the performed multicycling. Light blue represent desorbed state, whereas dark blue indicates adsorbed state*.

S5. Solvent and pH stability

In order to check the chemical stability of MIL-53(Al)-TDC towards different solvents and pH 1/pH 12 solutions, approximately 10 mg of MIL-53(Al)-TDC was suspended in 3 mL solvent each. After 24 h of stirring, the solid was recovered by centrifugation and dried (80 °C, 50 mbar). Subsequent PXRD analyses are illustrated in the Figures S4 and S5.

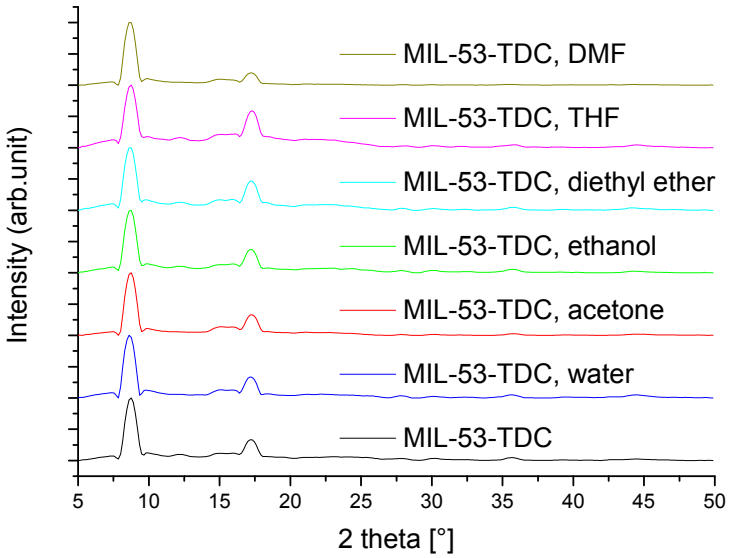

Figure S4 *PXRDs of MIL-53(Al)-TDC before and after 24 h of stirring in the stated solvent.*

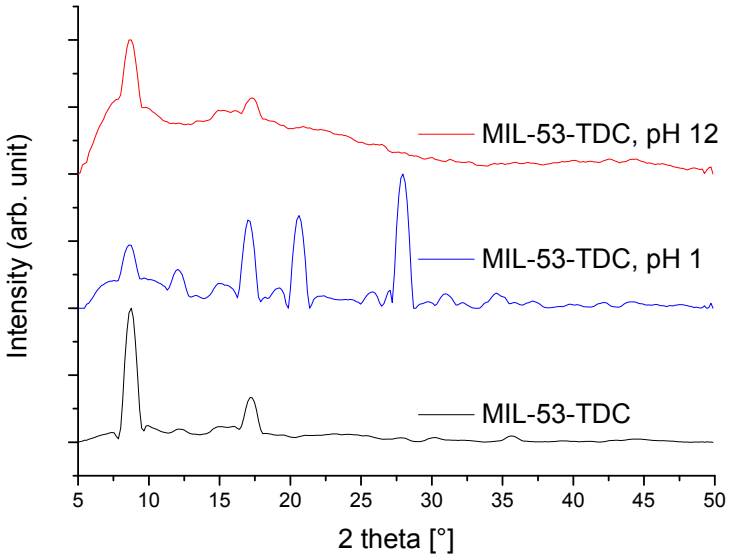

Figure S5 *PXRDs of MIL-53(Al)-TDC before and after 24 h of stirring in pH 1/pH 12 solutions (HNO_3 and NaOH used for pH adjustment).*

MIL-53(Al)-TDC seems to be highly stable towards organic solvents. None of the applied solvents seem to affect the crystallinity of the MIL-53(Al)-TDC phase. Figure S5 reveals that the compound loses crystallinity in pH 12, as the amorphous ratio in the pattern arises. After treatment in a pH 1 solution, MIL-53(Al)-TDC seems to be still present in the sample. However, the powder diffractogram shows various additional reflexes.

S6. Thermogravimetric Analysis (TGA)

TGA measurements were carried out on a *Netzsch TG209 F3 Tarsus* (NETZSCH, Selb, Germany) device under nitrogen atmosphere, ramping with 5 $Kmin^{-1}$ to target temperature (600 °C). Figure S6 shows the TGA curve of MIL-53(Al)-TDC obtained from $Al(OH)(ac)_2$.

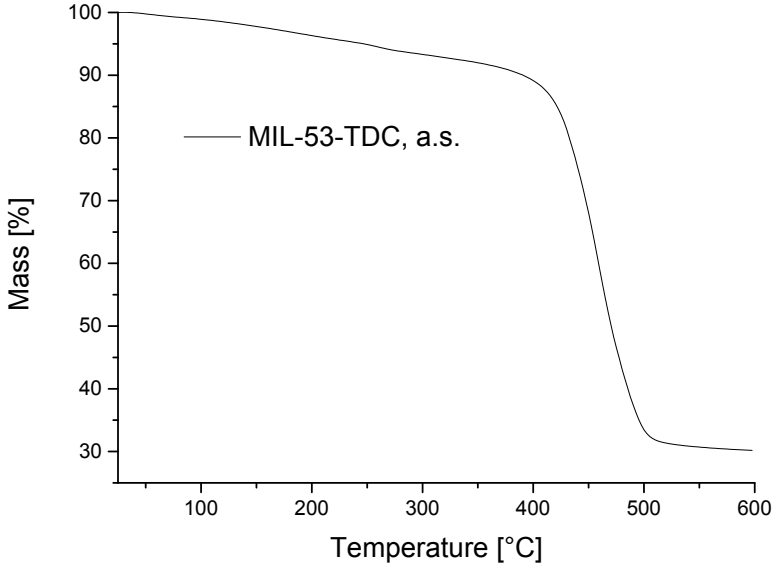

Figure S6 *TGA curve of MIL-53(Al)-TDC, revealing thermal stability up to at least 400 °C.*

The curve reveals thermal stability of the compound up to at least 400 °C, which is in very good accordance to Stock and co-workers, who reported the same value (cf. ESI† of Tschense *et al.*).[1]

S7. Elemental analysis

Elemental analysis was acquired on a *vario MICRO cube* (ELEMENTAR ANALYSENSYSTEME, Langenselbold, Germany).

Elemental analysis confirmed the composition of the as-synthesized product:

- **C** (meas.: 31.14%, calc. 31.04)
- **H** (meas.: 1.50%, calc. 2.17%)
- **S** (meas.: 13.21, calc. 13.81%)

The results are in good agreement with the thermogravimetric analysis.

S8. Infrared (IR) spectral analysis

Infrared spectra were acquired on a *Bruker Tensor 37 FT-IR* device. Figure S7 depict the IR spectra of MIL-53(Al)-TDC and the linker H_2TDC.

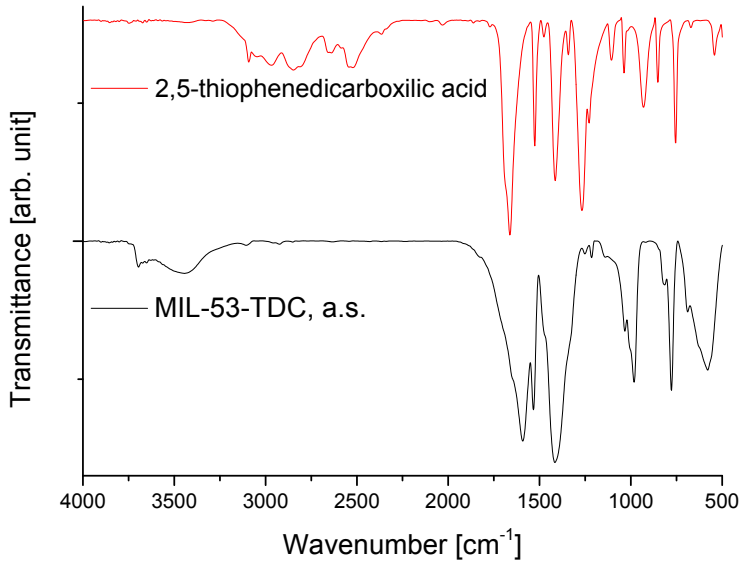

Figure S7 *Infrared spectra of MIL-53(Al)-TDC (black) and free linker 2,5-thiophenedicarboxylic acid (red).*

The IR spectrum of MIL-53(Al)-TDC is in very good accordance to Tschense *et al.*[1], who reported 1589 cm^{-1} and 1408 cm^{-1} for symmetric and asymmetric coordinating carboxylate groups. Stretching vibrations of the aromatic ring were consistently reported at $\nu_{C=C}$ = 1651 cm^{-1}, $\nu_{C=C}$ = 1531 cm^{-1} and ν_{C-S} = 690 cm^{-1}. That is good accordance to the prior report (cf. 1668 cm^{-1} for DMF, 1589 cm^{-1} and 1408 cm^{-1} for symmetric and asymmetric vibrations of carboxylate, and $\nu_{C=C}$ = 1651 cm^{-1}, 1531 cm^{-1} and ν_{C-S} = 690 cm^{-1} for the aromatic vibrations.[1]

Ancillary, a broad band around 3500 cm^{-1} can be observed, indicating H-bonds and incorporated water molecules inside the cavities. The band around 3685 cm^{-1} more pronounced than reported lately.[1] It is affected by μ-OH groups of the framework and therefore another distinctive band for the product. Additionally, we provide the IR spectrum of H_2TDC, which proves absence of unreacted linker molecules by absence of corresponding IR absorbance bands (e.g. absence of prominent band around 1280 cm^{-1}, present in the linker H_2BDC).

S9. Scanning electron microscopy (SEM)

For control of morphology we recorded SEM images using a *JEOL JSM-6510 Advanced electron microscope* (JEOL, Akishima, Japan) with a LaB_6 cathode at 5-20 keV. The microscope was equipped with a *Xflash 410* (BRUKER, Billerica, US) silicon drift detector. Figures S8-S11 show selected images of obtained samples out of varying Al-sources.

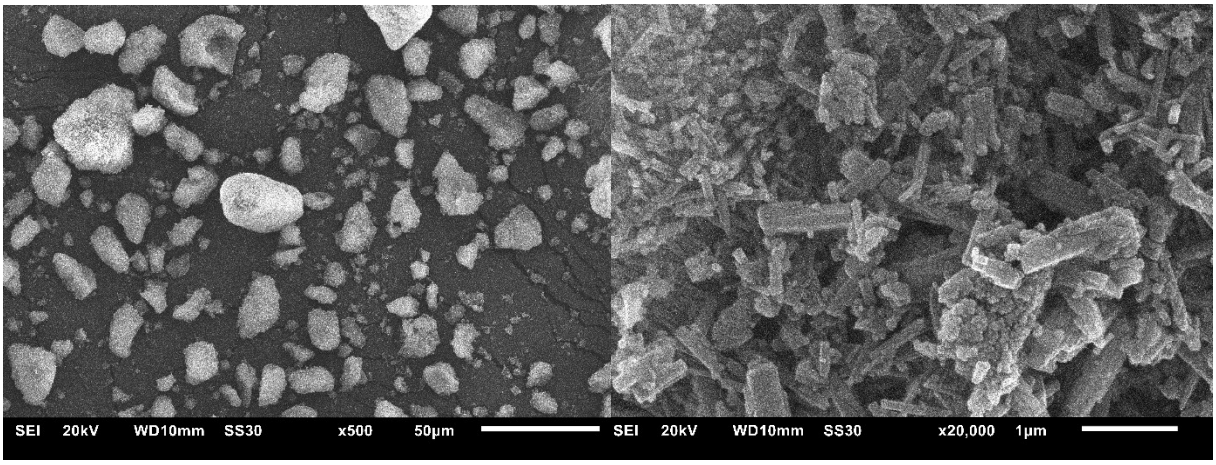

Figure S8 *SEM images of MIL-53(Al)-TDC obtained out of Al(OH)(ac)$_2$, left: overview of agglomerates, right: close-up.*

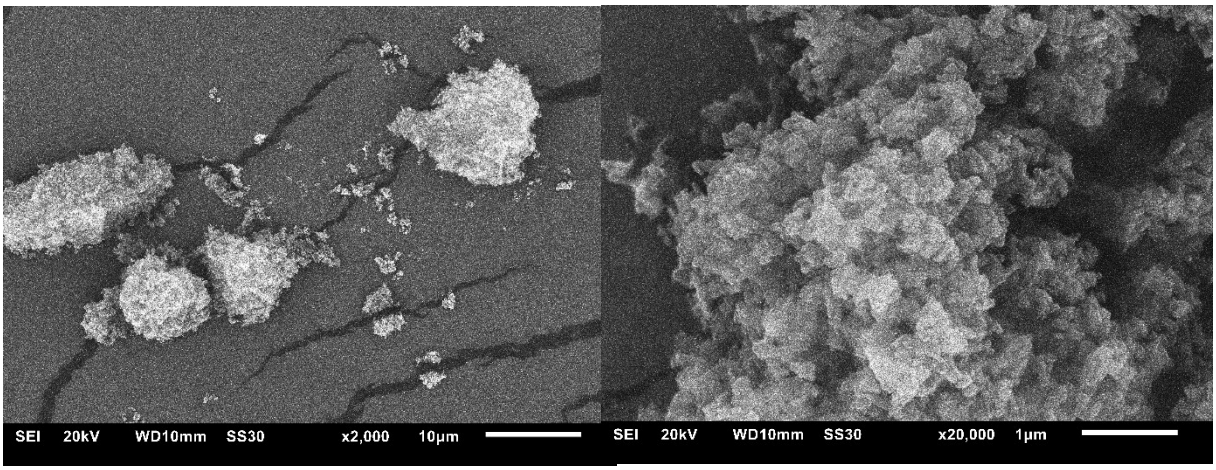

Figure S9 *SEM images of MIL-53(Al)-TDC obtained out of $AlCl_3$, left: overview of agglomerates, right: close-up.*

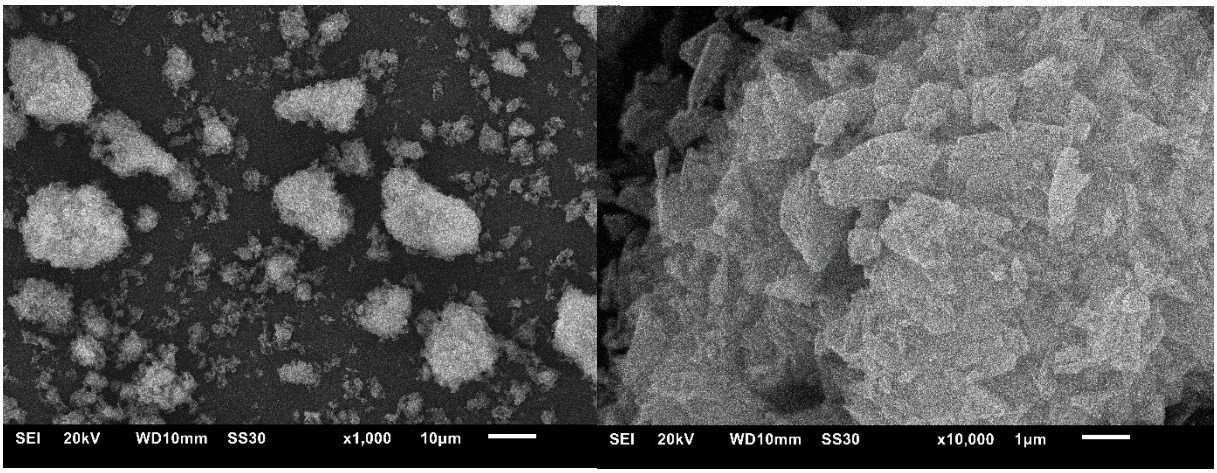

Figure S10 *SEM images of MIL-53(Al)-TDC obtained out of $Al_2(SO_4)_3$, left: overview of agglomerates, right: close-up.*

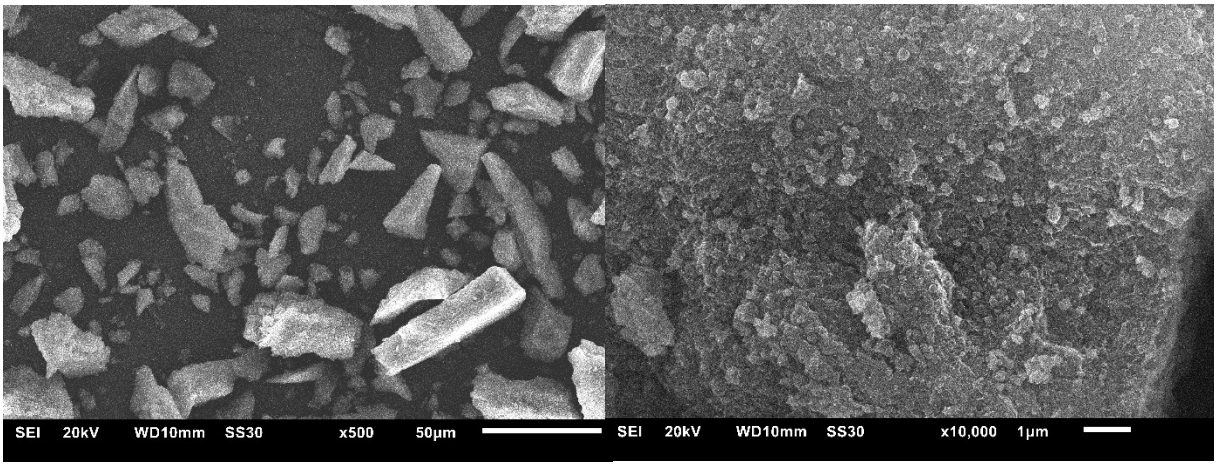

Figure S11 *SEM images of MIL-53(Al)-TDC obtained out of $NaAlO_2$, left: overview of agglomerates, right: close-up.*

All samples appear to be composed as agglomerates, which is typical for Al-based MOFs. The observation of different crystallite morphologies with the same PXRD pattern and comparable degree of crystallinity is evident. Certainly, all samples can be designated as uniform homogeneous MIL-53(Al)-TDC materials, nevertheless crystallite morphologies variegate with the applied Al-source. In comparison to the picture shown in the ESI† of Stock and co-workers,[1] the morphology of our material obtained from $Al(OH)(ac)_2$ seems to be most alike. Yet, morphology may also vary due to reflux syntheses in in the present cases shown above, compared to microwave solvothermal synthesis in the literature.

S10. Nitrogen sorption experiments (T = 77 K)

Surface areas (BET) were determined by nitrogen (purity 99.999%, 5.0) sorption experiments at 77 K using liquid nitrogen and performing on a *Quantachrome NOVA-4000e* (QUANTACHROME, Odelzhausen, Germany) instrument within a partial pressure range of $p/p_0 = 10^{-3}$-1 bar.

Each sample was degassed under vacuum (<10^{-2} mbar) at 150 °C for ca. 3 h, prior to measurement.

All surface areas (BET) were calculated from five adsorption points in the pressure range $p/p_0 = 0.005$-0.05 by applying Roquerol plots ($r > 0.998$). This range is indeed not recommended by IUPAC (International Union of Pure and Applied Chemistry) for BET surface determination, but rather suitable for microporous materials.[2]

Total pore volumes were calculated from the N_2 sorption isotherm at $p/p_0 = 0.95$. NLDFT calculations for the pore size distribution curves were done with the native *NovaWin 11.03* software using the 'N_2 at 77 K on carbon, slit pore, NLDFT equilibrium' model.

Figure S12 depicts the nitrogen sorption isotherm of MIL-53(Al)-TDC obtained out of $Al(OH)(ac)_2$ (that is the material used for multicycle stability experiments and further water sorption experiments, including affiliated calculations.).

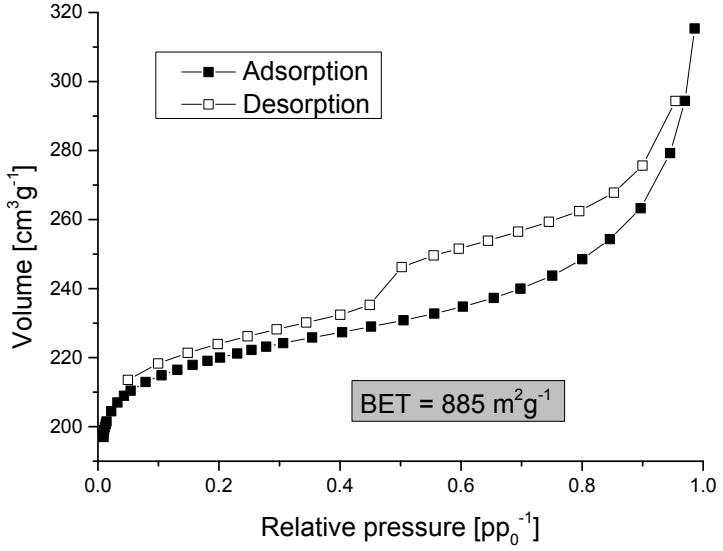

Figure S12 *Nitrogen sorption isotherms of MIL-53(Al)-TDC obtained out of Al(OH)(ac)$_2$.*

Figure S13 shows the isotherms collected from the samples derived from different Al-sources.

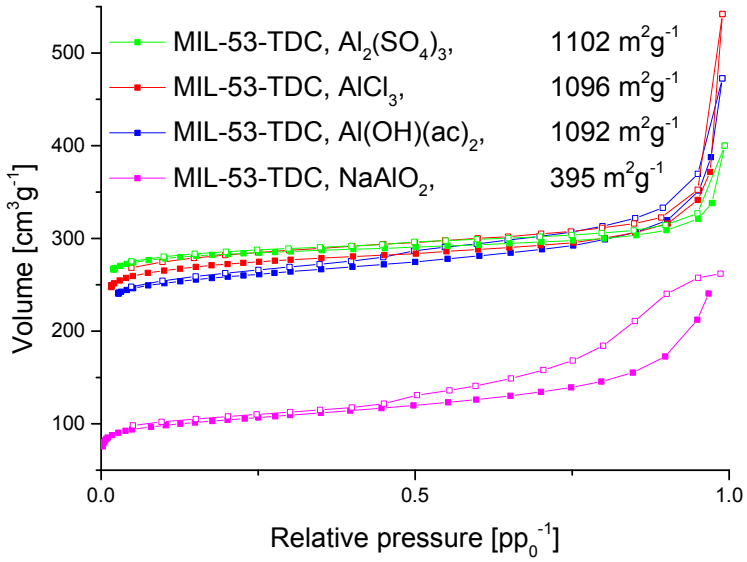

Figure S13 *Nitrogen sorption isotherms of MIL-53(Al)-TDC samples obtained out of varying Al-sources.*

The results show that although MIL-53(Al)-TDC was synthesized free from phase shift in all cases of Al-sources (cf. PXRD patterns in Figure S1), porosity varied. The reactant $NaAlO_2$ cannot compete with the other three starting materials, which seem to be more or less in the same range of porosity. Table S3 concludes the porosity parameters derived from nitrogen sorption isotherms (cf. Figure S13) of MIL-53(Al)-TDC samples obtained out of varying Al-sources.

Table S3 *Porosity parameters of different MIL-53(Al)-TDC samples obtained out of varying Al-sources, determined with nitrogen sorption (77 K) and stated calculation methods.*

Al-source	S_{BET} $[m^2g^{-1}]^a$	$S_{BET\,(micro)}$ $[m^2g^{-1}]^b$	V_{total} $[cm^3g^{-1}]^c$	V_{micro} $[cm^3g^{-1}]^d$
$Al(OH)(ac)_2 \cdot x\ H_2O$	885, 1092	800, 965	0.41, 0.52	0.30, 0.43
$NaAlO_2$	395	275	0.37	0.11
$Al(SO)_4 \cdot 18H_2O$	1102	1041	0.46	0.41
$AlCl_3 \cdot 6\ H_2O$	1096	1002	0.49	0.38
$AlCl_3$, ref. [1] *	1150	Not specified	Not specified	0.48

[a] Specific surface areas (S_{BET}) were determined by five adsorption points of nitrogen sorption isotherms in the range $0.005 < pp_0^{-1} < 0.05$. [b] Micropore areas were determined by t-plot method with De Boer model in the range $0.2 < pp_0^{-1} < 0.4$. [c] Total pore volumes (V_{total}) were calculated at $pp_0^{-1} = 0.9$. [d] Micropore volumes (V_{micro}) were calculated by NLDFT method (carbon, slit pore, nitrogen, 77 K). * Determined at $pp_0^{-1} = 0.5$.

S11. Argon sorption experiments (T = 87 K)

Argon (purity 99.999%, 5.0) sorption experiments were performed at 87 K using a *Quantachrome CryoCooler* (QUANTACHROME, Odelzhausen, Germany) for appropriate adjustment of T = 87 K and performing on a *Quantachrome Autosorb iQ MP* (QUANTACHROME, Odelzhausen, Germany) instrument with within a partial pressure range of $p/p_0 = 10^{-7}$-1 bar.

Each sample was degassed under vacuum (<10^{-5} mbar) at 150 °C for ca. 3 h, prior to measurement. All surface areas (BET) were calculated from five adsorption points in the pressure range $0.005 < pp_0^{-1} < 0.05$

Additionally, we carried out argon sorption measurements (87 K) which is rather rare, but recommended for microporous materials.[2] While nitrogen sorption (cf. Figure S11) often overestimates BET areas of (especially micro- to mesoporous) MOFs,[2,3,4] it determined a specific surface area of BET = 885 m^2g^{-1} and 0.41 cm^3g^{-1} pore volume (NLDFT, carbon, slit pore, nitrogen, 77 K). Argon sorption revealed a surface area of BET = 827 m^2g^{-1} and 0.35 cm^3g^{-1} pore volume (NLDFT, carbon, slit pore, argon, 87 K) and 0.27 cm^3g^{-1} micropore volume (t-plot method, De Boer model). It has to be noted that BET calculation is usually performed in a pressure range $0.05 < pp_0^{-1} < 0.3$, but its applicability also works for microporous materials in a lower range (here: $0.005 < pp_0^{-1} < 0.05$).[3,5]

Argon sorption was carried out exemplarily for a sample obtained out of $Al(OH)(ac)_2$, from which the isotherm is depicted in Figure S14. The shape of isotherm is typical for microporous material, a Type-I isotherm with steep increase at relative pressures of $pp_0^{-1} < 0.1$.

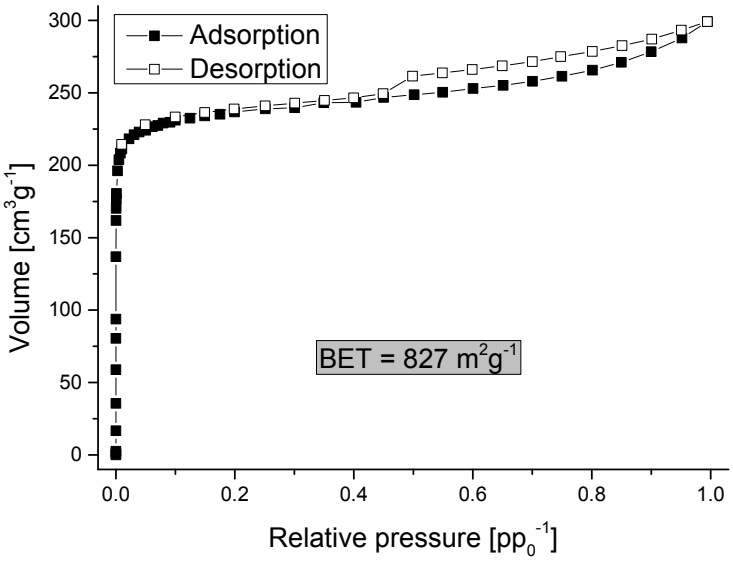

Figure S14 *Argon sorption isotherm (87 K), exhibiting typical isotherm Type-I appearance for microporous materials.*

S12. Water sorption and isosteric heat of adsorption

All water sorption isotherms (25, 40, 60 °C) were measured with a *Quantachrome VStar4* (QUANTACHROME, Odelzhausen, Germany) within a partial pressure range of $p/p_0 = 10^{-3}$-0.9 bar. Each sample was degassed under vacuum (<10^{-5} mbar) at 150 °C for ca. 3 h, prior to measurement. The acquired data were fit with native *VersaWin™ 1.0* software.

Figure S15 illustrates the water sorption isotherms of different samples MIL-53(Al)-TDC.

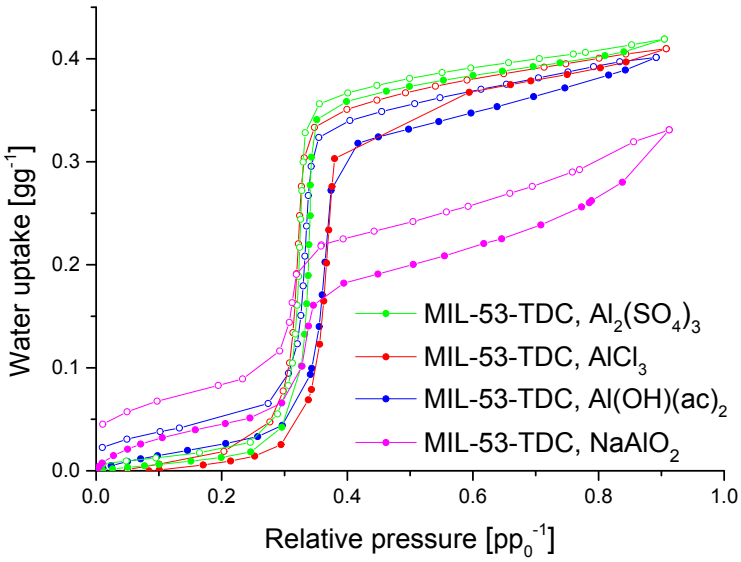

Figure S15 *Water sorption isotherms of MIL-53(Al)-TDC samples obtained out of varying Al-sources.*

Obviously, the influence of the Al-source occurs on smaller scales for three of the four tested Al-sources (i.e. $Al_2(SO_4)_3$, $Al(OH)(acetate)_2$ and $AlCl_3$), which correlates with N_2 sorption results (cf. Table S3). However, hystereses differ even among the named materials, indicating probably residual or coordinated anions of the Al-sources that bias during ad- and desorption.

The isosteric heat of adsorption was determined directly from the measurements at 25 °C, 40 °C and 60 °C (Figure 3 in the full paper), and this data was fitted by a thermodynamic model according to *Van't Hoff* (eqn (1)).[6]

$$\frac{\Delta H_{ads}(X,T)}{RT^2} = -\left(\frac{\partial \ln p}{\partial T}\right)_{X(p,T)} \qquad (1)$$

For the broadest range of adsorbed amount, the heat of adsorption is constant at around 2.6 kJ g^{-1}.

Water uptake capacity as a function of heat rejection can be seen in Figure 6 in the full paper. Sensitivity of uptake capacity towards desorption temperature and condenser temperature is also given in the full paper in Figure 7.

S13. Multiycle stability tests

Water cycling stabilities were examined in a *Setaram™ TGA-DSC-111* (SETARAM, Caluire, France) on powdered samples. A humidified argon gas flow (40 °C, 76.3% relative humidity) was generated by a *Setaram™ WetSys* (SETARAM, Caluire, France) humidity controller and passed through the sample chamber, while the temperature of the sample was varied and the mass of the adsorbent was monitored. For the multi-cycle ad-/desorption experiments, the temperature of the sample was varied between 40 °C and 140 °C with a cycle time of 5 h.

The cycling results of the firs 40 cycles are depicted in Figure S16.

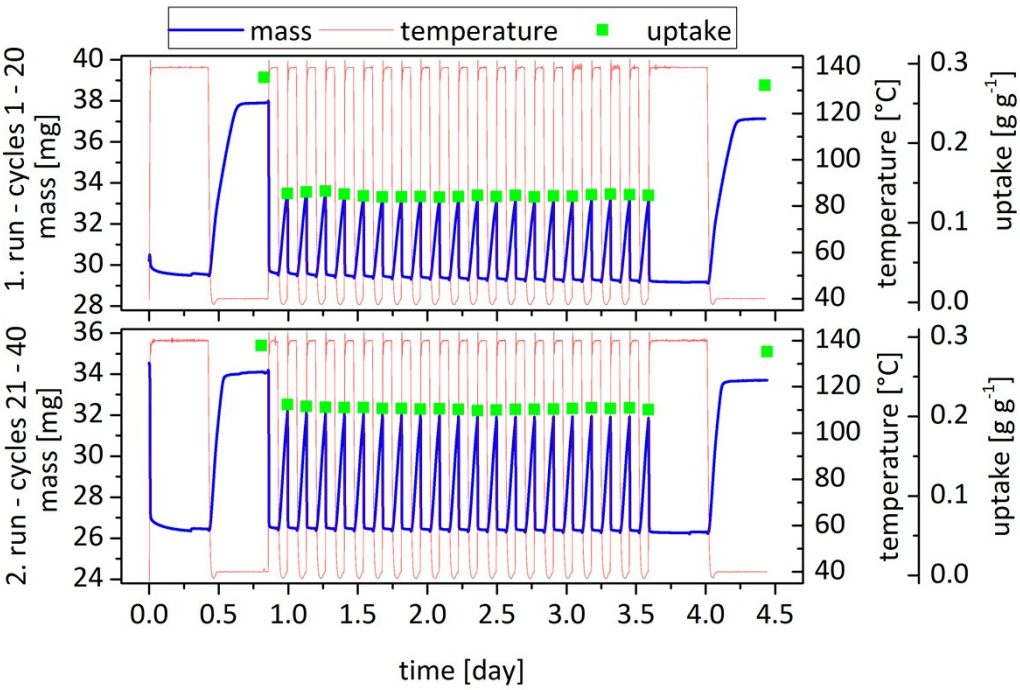

Figure S16 *Multicycle water stability tests (40 cycles). Blue: sample mass [mg], red: temperature [°C], green: uptake [gg^{-1}].*

To fit the experimental data, a recently proposed [7,8] weighted Dual-Site Langmuir (wDSL) approach was used:

$$X(p,T) = X_L(1 - w(p,T)) + X_U(p,T)w(p,T) \quad (2)$$

$$X_L(p,T) = X_{L,\infty}\frac{b_L p}{1 + b_L p} \quad (3)$$

$$X_U(p,T) = X_{U,\infty}\frac{b_U p}{1 + b_U p} + b_H p \quad (4)$$

$$b_\alpha = b_{\alpha,\infty}\exp\left(\frac{E_\alpha}{RT}\right), \alpha = L,U,H \quad (5)$$

$$w(p,T) = \left(\frac{\exp\left(\frac{\ln(p) - \ln\left(p_{step}(T)\right)}{\sigma(T)}\right)}{1 + \exp\left(\frac{\ln(p) - \ln\left(p_{step}(T)\right)}{\sigma(T)}\right)}\right)^\gamma \quad (6)$$

$$\sigma(T) = \chi_1\exp\left(\chi_2\left(\frac{1}{T_0} - \frac{1}{T}\right)\right) \quad (7)$$

$$p_{step}(T) = p_{step,0}\exp\left(\frac{-H_{Step}}{R}\left(\frac{1}{T_0} - \frac{1}{T}\right)\right) \quad (8)$$

, wherein the water uptake at a certain pressure and temperature *X(p,T)* is calculated from two Langmuir-terms (X_L and X_U), representing the adsorption before and after the step in the uptake. *w(p,T)* is a weighting function that depends on the pressure *p*, the temperature *T* and the pressure p_{step} at which the uptake step occurs. Further symbols X_∞, b_α, E_α and $\chi_{1,2}$ represent fit parameters.

Figure S17 gives a graphical illustration of thermodynamic evaluation of MIL-53(Al)-TDC (cf. Fig. 1).

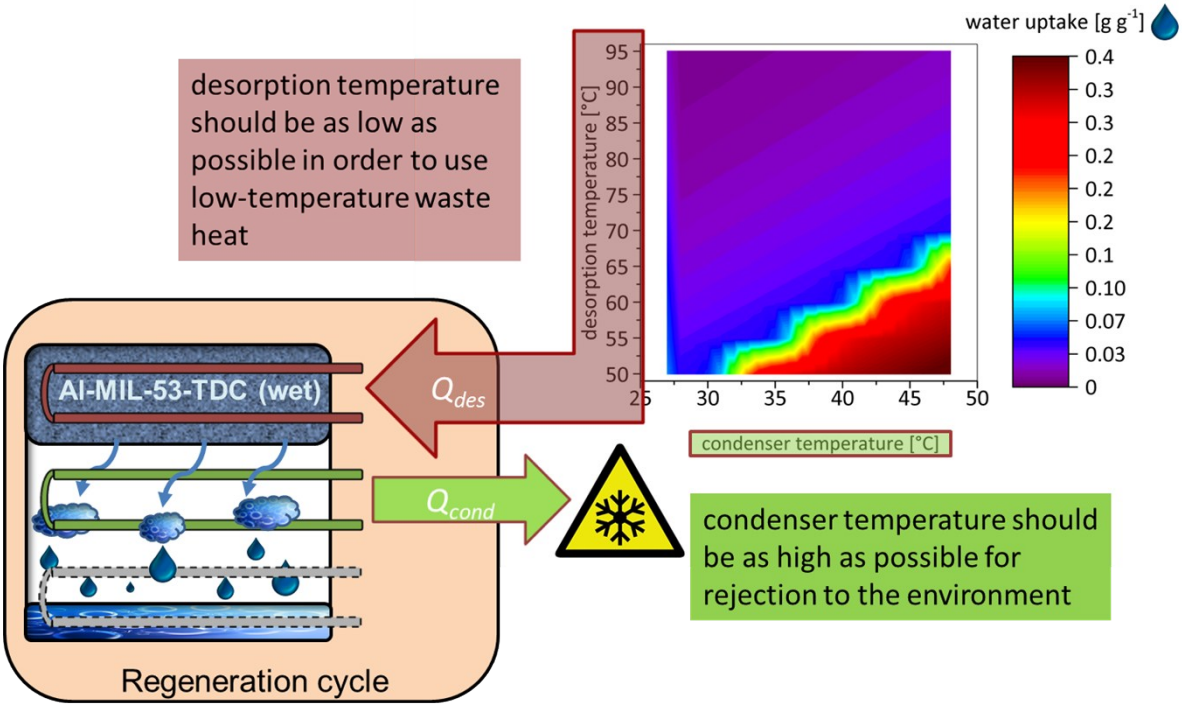

Figure S17 *Illustration of the thermodynamic evaluation of MIL-53(Al)-TDC, which yields preferably low desorption temperatures at comparably good high condenser temperatures and reasonable water uptake capacities of ~0.3 g g^{-1}.*

S14. References

1 C. W. L. Tschense, N. Reimer, C.-W. Hsu, H. Reinsch, R. Siegel, W.-J. Chen, C.-H- Lin, A. Cadiau, C. Serre, J. Senker and N. Stock, *Z. Anorg. All. Chem.*, 2017, **21**, 1600-1608.

2 M. Thommes, K. Kaneko, A. V. Neimark, J. P. Olivier, F. Rodriguez-Reinoso, J. Rouquerol and K. S. Sing, *Pure Appl. Chem.*, 2015, **87**, 1051-1069.

3 D. A. Gómez-Gualdrón, P. Z. Moghadam, J. T. Hupp, O. K. Farha and R. Q. Snurr, *J. Am. Chem. Soc.*, 2016, **138**, 215-224.

4 T. C. Wang, W. Bury, D. A. Gómez-Gualdrón, N. A. Vermeulen, J. E. Mondloch, P. Deria, K. Zhang, P. Z. Moghadam, A. A. Sarjeant, R. Q. Snurr, J. F. Stoddart, J. T. Hupp and O. K. Farha, *J. Am. Chem. Soc.*, 2015, **137**, 3585-3591.

5 K. S. Walton and R. Q. Snurr, *J. Am. Chem. Soc.*, 2007, **129**, 8552-8556.

6 D. M. Ruthven, Principles of adsorption and adsorption processes, Wiley, New York, 1984.

7 M. Hefti, L. Joss, Z. Bjelobrk and M. Mazzotti, *Faraday Discuss.*, 2016, **192**, 153-179.

8 S.-J. Ernst, M. Baumgartner, D. Fröhlich, H.-J. Bart and S. K. Henninger, *Chem-Ing-Tech.*, 2017, **89**, 1650-1660.